

Practical quantum federated learning and its experimental demonstration

Zhi-Ping Liu,^{1,2,*} Xiao-Yu Cao,^{1,2,*} Hao-Wen Liu,^{1,2,*} Xiao-Ran Sun,^{1,2}
Yu Bao,^{1,2} Yu-Shuo Lu,^{1,2} Hua-Lei Yin,^{2,1,3,†} and Zeng-Bing Chen^{1,‡}

¹*National Laboratory of Solid State Microstructures and School of Physics,
Collaborative Innovation Center of Advanced Microstructures, Nanjing University, Nanjing 210093, China*
²*School of Physics and Beijing Key Laboratory of Opto-electronic Functional Materials and Micro-nano Devices,
Key Laboratory of Quantum State Construction and Manipulation (Ministry of Education),
Renmin University of China, Beijing 100872, China*

³*Beijing Academy of Quantum Information Sciences, Beijing 100193, China*

(Dated: January 23, 2025)

Federated learning is essential for decentralized, privacy-preserving model training in the data-driven era. Quantum-enhanced federated learning leverages quantum resources to address privacy and scalability challenges, offering security and efficiency advantages beyond classical methods. However, practical and scalable frameworks addressing privacy concerns in the quantum computing era remain undeveloped. Here, we propose a practical quantum federated learning framework on quantum networks, utilizing distributed quantum secret keys to protect local model updates and enable secure aggregation with information-theoretic security. We experimentally validate our framework on a 4-client quantum network with a scalable structure. Extensive numerical experiments on both quantum and classical datasets show that adding a quantum client significantly enhances the trained global model’s ability to classify multipartite entangled and non-stabilizer quantum datasets. Simulations further demonstrate scalability to 200 clients with classical models trained on the MNIST dataset, reducing communication costs by 75% through advanced model compression techniques and achieving rapid training convergence. Our work provides critical insights for building scalable, efficient, and quantum-secure machine learning systems for the coming quantum internet era.

Deep learning has achieved remarkable success across various fields [1], including disease diagnosis [2], autonomous driving [3], and tackling critical scientific challenges [4, 5]. In particular, the advent of large language models [6, 7] has underscored the influence of empirical scaling laws related to model and dataset size [8]. The effectiveness of large language models like GPT-4 and Llama 3 stems largely from access to massive public datasets. However, high-quality private data, such as medical data and behavior data of users [9, 10], are often isolated among clients, complicating their integration into centralized learning systems.

To address the challenges of data privacy, federated learning has emerged as a decentralized paradigm, enabling collaborative model training while keeping client data local [11, 12]. This method has been effectively applied in privacy-sensitive areas, including healthcare [13], the Internet of Things [14], and personalized recommendations [15]. Concurrently, quantum machine learning has emerged as a transformative field [16–18], combining machine learning with quantum theory to exploit the advantages of both domains. Quantum federated learning [19] (QFL) extends federated learning into the realm of quantum machine learning, consisting of a cloud server and multiple clients that access quantum resources.

To further the development of QFL, several frameworks [20–22] have been proposed to enhance communication efficiency with quantum machine learning models, such as variational quantum circuits [23] or quantum neural networks (QNNs), which are considered promising models for the noisy intermediate-scale quantum era [24]. While communication efficiency is critical, ensuring data privacy remains a more significant concern in QFL. Although clients do not share raw local data, gradient inversion attacks [25] can still expose private information through shared gradients or model updates. Recent efforts have sought to mitigate these attacks through designing sophisticated quantum algorithms [26–29] or involving differential privacy techniques [30]. However, many of these approaches require extensive quantum resources beyond current capabilities or fail to offer perfect data privacy. Consequently, there is an ongoing demand for a practical QFL framework that provides quantum security for data privacy in the coming era of large-scale quantum computing.

Quantum networks enable applications that surpass the classical ones [31–33] and many tasks have been demonstrated on quantum networks, which show quantum advantages [34–38]. Specifically, quantum key distribution (QKD) serves as a foundational component of the quantum internet [31], ensuring confidentiality of information transmission with information-theoretic security. With great progress made in recent years [39–45], QKD has laid the groundwork for integrating deep learning algorithms into quantum networks, paving the way for more practical privacy-preserving machine learning

* These authors contributed equally.

† hlyin@ruc.edu.cn

‡ zbchen@nju.edu.cn

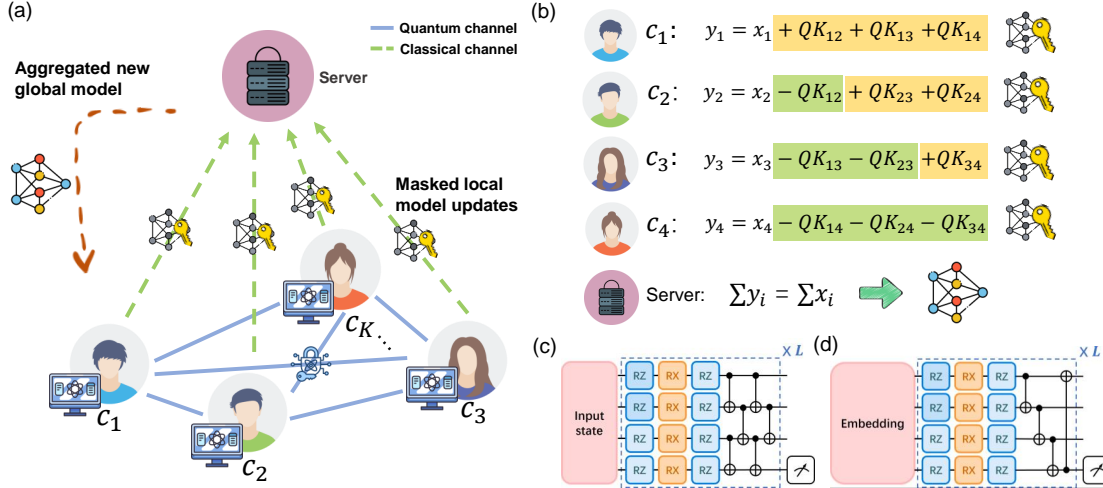


Fig 1. **Schematic of the QuNetQFL Framework.** (a) The QuNetQFL framework employs a fully connected quantum network among K clients, where each client uses QKD to securely exchange quantum secure keys with others, enabling pairwise masking of local model updates. Only these masked updates are sent to the server through classical channels, preserving client privacy. The server aggregates the updates to form an unmasked global model parameter, which is then redistributed to all clients. (b) Masked secure aggregation in a four-client setup. Here, x_i represents the raw local updates and y_i the masked updates. The server simply sums the masked updates to obtain the decrypted global model update. (c) and (d) Two types of QNN representations with hardware-efficient ansatzes used in the study.

systems. The rapid development of quantum networks presents a unique opportunity for advancing QFL [46].

In this work, we propose QuNetQFL, a practical quantum federated learning framework natively implemented on quantum networks, ensuring secure aggregation of model updates with information-theoretic security. Our framework is designed for a cross-silo QFL scenario, where a limited number of organizations, such as those in finance and healthcare, collaborate using reliable communications and relatively abundant quantum and classical resources. This setting demands stringent privacy and learning performance requirements [47], matching the needs of clients in quantum networks. Instead of using costly homomorphic encryption [48–50], QuNetQFL utilizes secure keys generated by QKD to create pairwise masks for clients’ local model updates, employing only lightweight encryption. This enables the server to receive masked updates, thereby performing secure model aggregation without exposing individual client data (see Fig. 1 for an illustration). Compared to classical secure aggregation schemes [51], our approach achieves genuine one-time pad-based masking through QKD techniques, offering a significant quantum security advantage in the evolving landscape of quantum computing.

Furthermore, we validate our framework by employing four-phase measurement-device-independent (MDI) QKD [43] in a four-client quantum network. Using a Sagnac interferometer for phase stability, we present a proof-of-principle demonstration of a multi-user quantum network over 6 kilometers of optical fiber, achiev-

ing a secret key rate exceeding 32.8 kbps. This structure is highly scalable, allowing the number of clients to adjust without altering the core network design, making it well-suited for multi-client quantum networks and QFL tasks. Leveraging the generated quantum secret keys, we implement QuNetQFL and evaluate its performance through extensive experiments on both quantum and real-world classical datasets. We also investigate the impact of non-independent and identically distributed (non-IID) data and the addition of clients to the framework. Notably, adding one quantum client significantly enhances the global model’s ability to classify multipartite entangled and quantum magic datasets, demonstrating the framework’s ability to detect essential quantum communication and computation resources in a privacy-preserving, distributed scenario. Additionally, we achieve comparable performance in classifying handwritten digit images from the MNIST dataset using QNNs under both IID and non-IID data distributions. Simulations further show the framework’s scalability to 200 clients using classical learning models on the MNIST dataset, with fast convergence and improved communication efficiency when combined with advanced model compression techniques. Our work addresses the critical need for a practical QFL framework that efficiently operates within current quantum resource constraints while ensuring quantum security in the era of large-scale quantum computing.

Results

Framework of QuNetQFL. The fundamental QFL

setup consists of a central server and K quantum clients. Each client possesses a local dataset $D_k = \{(\rho_k^i, \mathbf{y}_k^i)\}_{i=1}^{n_k}$, where ρ_k^i denotes a quantum state and \mathbf{y}_k^i is the corresponding label. The dataset D_k can be a native quantum dataset or a dataset generated through encoding classical data into quantum states [52], given by $\rho_k^i = \rho(\mathbf{x}_k^i)$ with $\mathbf{x}_k^i \in \mathbb{R}^d$. In the t -th communication round, the server sends the global QNN parameters $\boldsymbol{\theta}^{t-1} \in \mathbb{R}^M$ to the clients. Each client then trains a local model $\boldsymbol{\theta}_k^t$ by minimizing the local loss function $\mathcal{L}(\boldsymbol{\theta}_k^t)$ that captures the error between predictions and true labels of its local dataset. After local training, each client computes an update $\Delta\boldsymbol{\theta}_k^t = \boldsymbol{\theta}_k^t - \boldsymbol{\theta}^{t-1}$ based on its local loss, which is sent to the server. The server aggregates these updates using a weighted sum to form the global model update:

$$\Delta\boldsymbol{\theta}^t = \sum_{k=1}^K \frac{n_k}{N} \Delta\boldsymbol{\theta}_k^t, \quad (1)$$

where $N = \sum_{k=1}^K n_k$ is the total number of data instances across all involved clients. This aggregated update is then used to update the global model parameters with $\boldsymbol{\theta}^t = \boldsymbol{\theta}^{t-1} + \Delta\boldsymbol{\theta}^t$. While this setup preserves data privacy by sharing only model updates, it remains vulnerable to gradient attacks that could reveal client information.

To ensure secure updates, QuNetQFL employs QKD to achieve a masking-based secure aggregation scheme (see Fig. 1 (b) for an illustration). This approach leverages a fully connected quantum network for secure quantum key exchanges between all participating clients. In the t -th communication round, a subset of clients $\mathcal{S}^t \subset \{1, 2, \dots, K\}$ is selected to participate by the server. After achieving local training, clients in \mathcal{S}^t exchange quantum secret keys pairwise through the pre-negotiated QKD protocol in the quantum network, denoted by $\text{QK}_{i,j}^t$ for each client pair (i, j) . In each communication round, the keys $\text{QK}_{i,j}^t$ exchanged between client pairs are represented as $(M \times q)$ -bit binary strings, where M is the model size and q specifies the quantization bit length. The cost of quantum secure keys in the QuNetQFL scales as $\mathcal{O}(K^2 M)$. To integrate QKD into the framework, quantization is used to compress large models, balancing the communication cost (cost of quantum keys) with model training performance. Each key is treated as a vector with M entries, where each entry is a q -bit signed integer, i.e., $\text{QK}_{i,j}^t \in \mathbb{Z}^M$, with the k -th entry $\text{QK}_{i,j}^t[k] \in [-(2^{q-1} - 1), (2^{q-1} - 1)]$.

We note that $\text{QK}_{i,j}^t = \text{QK}_{j,i}^t$ represents symmetric key sharing between each via QKD protocols. These keys are then used as a one-time padding mask as follows. The i -th client in \mathcal{S}^t computes the quantized weighted difference $\Delta\boldsymbol{\theta}_i^t = \boldsymbol{\theta}_i^t - \boldsymbol{\theta}^{t-1}$, masks it with the shared

secret keys, and uploads the masked local update:

$$\Delta\tilde{\boldsymbol{\theta}}_i^t = [Q^q(p_i^t \cdot \Delta\boldsymbol{\theta}_i^t) + \mathbf{m}_i^t] \bmod 2^q, \quad (2)$$

where $\mathbf{m}_i^t = \sum_{j \in \mathcal{S}^t, i \neq j} (-1)^{i > j} \text{QK}_{i,j}^t$, $p_i^t = n_i/N^t$ with $N^t = \sum_{i \in \mathcal{S}^t} n_i$ and $Q^q(\cdot)$ is the q -bit quantization function. The server aggregates the updates by summing the quantized values from all selected clients:

$$\Delta\boldsymbol{\theta}^t = \left[\sum_{i \in \mathcal{S}^t} \Delta\tilde{\boldsymbol{\theta}}_i^t \right] \bmod 2^q \quad (3)$$

$$= \left[\sum_{i \in \mathcal{S}^t} Q^q(p_i^t \cdot \Delta\boldsymbol{\theta}_i^t) \right] \bmod 2^q, \quad (4)$$

where an essential property that $[\sum_{i \in \mathcal{S}^t} \mathbf{m}_i^t] \bmod 2^q = 0$ is utilized. This aggregation process, combined with quantization and masking, ensures that the updates remain private. Finally, the server updates the global model parameters as follows:

$$\boldsymbol{\theta}^t = \boldsymbol{\theta}^{t-1} + D^q(\Delta\boldsymbol{\theta}^t), \quad (5)$$

where $D^q(\cdot)$ is the de-quantization function, and the quantization imprecision is $\mathcal{O}(1/2^q)$. The detailed pseudocode for this framework is given in Methods (see Algorithm 1).

This quantum-secured aggregation approach provides perfect privacy against gradient attacks, supporting secure and scalable QFL across distributed networks. The theoretical convergence analysis for QuNetQFL is provided in the supplementary information, offering both convergence guarantees and practical guidance for training, highlighting its practical advantages.

Security analysis. (a) Threat model. We adopt a commonly used threat model in federated learning. All clients and the cloud server are considered *honest-but-curious*. That is, while they faithfully follow the prescribed protocol, they may attempt to infer other clients' local datasets from individual local model updates. In this context, we are not addressing the extreme scenario, which is also highly impractical, considering the numerous geographically distributed clients where only one client is honest, and all other clients conspire with the cloud server. Our scheme excludes this extreme collusion, as in current research [53]. If the server colludes with all but one of the clients during secure sum computation, the data of the colluding clients can be reliably removed from the sum, exposing the honest client's data. (b) Security guarantees. Our scheme is designed to safeguard each client's local dataset from other clients, the cloud server, and potential third-party attackers. However, protecting the global model is not the goal of this work.

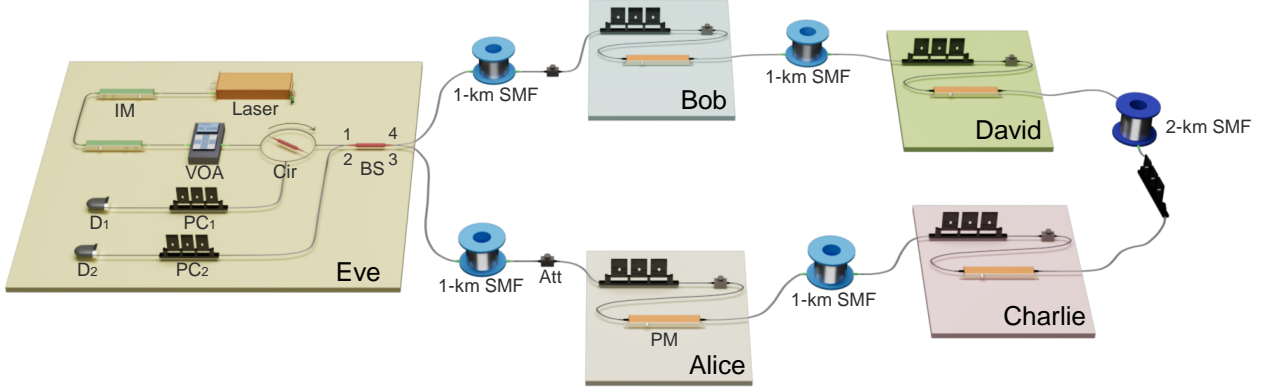


Fig 2. **Experimental setup of the quantum network.** At Eve’s site, a continuous-wave laser source is employed with two intensity modulators (IM) and a variable optical attenuator (VOA) to produce weak coherent pulses. Four clients (Alice, Bob, Charlie, and David) are interconnected in the Sagnac loop. When any pair of clients need to establish secret keys, Eve injects the pulses into the loop via a circulator (Cir) and a 50 : 50 beam splitter (BS). Upon reaching the designated clients, phase modulators (PMs) are employed to add phase to the pulses. After modulation, the two pulse trains interfere at Eve’s BS, where interference results are detected by two superconducting nanowire single-photon detectors (D_1 and D_2). This structure includes 1-km single-mode fibers (SMFs) between Alice and Eve, Bob and Eve, Alice and Charlie, and Bob and David, while a 2-km SMF connects Charlie and David. Attenuators (Att) are placed between Alice and Eve, and between Bob and Eve, to adjust channel losses. Polarization controllers (PCs) are used to align polarization in the loop.

TABLE I. **Summary of key rates (bit/pulse).** A, B, C, and D represent Alice, Bob, Charlie, and David, respectively.

3-client		4-client			
Client pair	Key rate	Client pair	Key rate	Client pair	Key rate
AB	2.30×10^{-3}	AB	2.40×10^{-3}	BC	4.46×10^{-4}
AC	3.76×10^{-4}	AC	3.56×10^{-4}	BD	3.66×10^{-4}
AD	4.59×10^{-4}	AD	4.30×10^{-4}	CD	3.28×10^{-4}

In QuNetQFL protocol, assume that in t -th round, a subset of total ordered clients \mathcal{C}^t is randomly sampled by the server, the index set of clients contained in \mathcal{C}^t is \mathcal{S}^t . For $i \in \mathcal{S}^t$ and $c_i \in \mathcal{C}^t$ have a q -bit quantized local update vector $Q^q(\Delta\theta_i^t)$, where its k -th entry $Q^q(\Delta\theta_i^t)[k]$ is a q -bit signed integers. Then each selected client $c_i \in \mathcal{C}^t$ adds the keys distributed under quantum networks, as the one-time pad, to pair-wisely mask it and obtain the masked vector $\tilde{\Delta\theta}_i^t$ as shown in Eq. (2). Note that each $\text{QK}_{i,j}^t[k]$ is a q -bit key distributed between client i and client j under quantum networks, which is truly random and secret. And $m_i^t[k]$ is also a q -bit truly random mask, which can be regarded as a q -bit signed integer. The result $\tilde{\Delta\theta}_i^t[k]$ is also a q -bit integer, which is perfectly masked. Thus, each client can mask their model to preserve their privacy from other clients and the server.

Experimental quantum network. To experimentally generate quantum secure keys for demonstrating QuNetQFL with 3 or 4 clients, we established a quantum network with five participants. This includes four clients, Alice, Bob, Charlie, and David, who potentially require

quantum secret keys for collaborative training, and one party, the untrusted Eve, responsible for measuring interference results, as shown in Fig. 2. Through this quantum network, each client pair can securely share quantum secret keys.

Here, we take the key generation process of MDI QKD between Alice and Bob as an example, which applies similarly to other client pairs. The system frequency is 100 MHz. The relevant protocol description can be found in Methods. In Eve’s site, to prepare weak coherent pulses with an extinction ratio exceeding 30 dB, two intensity modulators are utilized to chop the continuous light from a narrow linewidth continuous-wave laser source (NKT E15). Eve then sends the pulses into the loop after passing through a circulator and a 50 : 50 beam splitter (BS). In the loop, two clients modulate the pulse train with phase modulators. Note that users only modulate one pulse train. Specifically, Alice only modulates the clockwise pulses and Bob only modulates the counterclockwise pulses. Then, the two pulses interfere at Eve’s BS, and Eve records corresponding detection events by D_1 and D_2 . The detection efficiencies of D_1

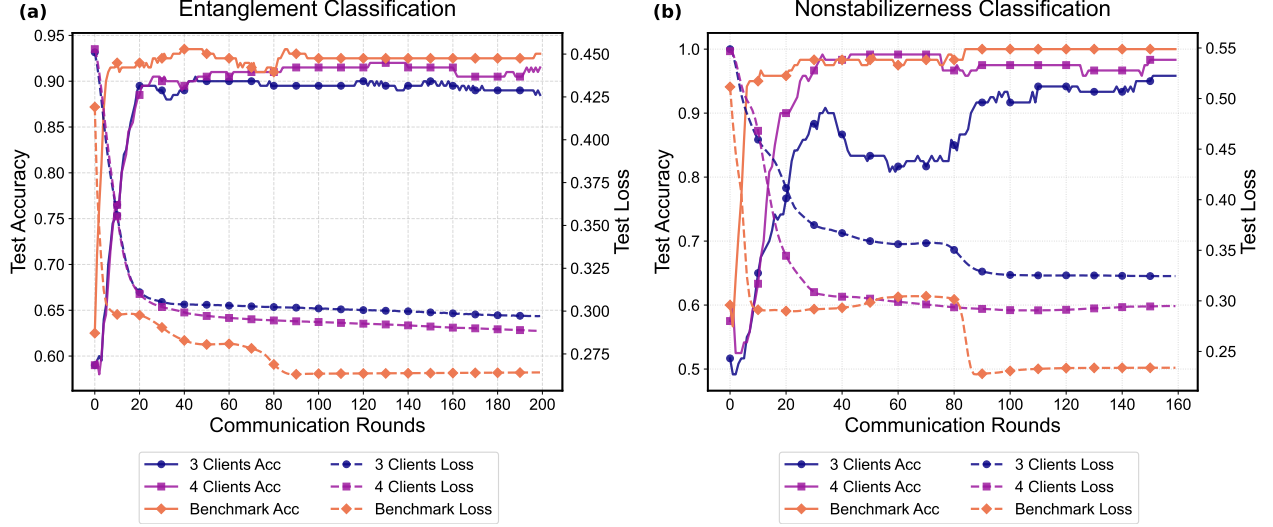


Fig 3. **Performance of QuNetQFL on quantum state classification using QNN.** (a) Entanglement classification: final test accuracies are 88.5% with three clients, 91.5% with four clients, and 93% for the benchmark. (b) Nonstabilizerness classification: final test accuracies are 95.8% with three clients, 98.3% with four clients, and 100% for the benchmark. These two tasks used 16-bit quantization ($q = 16$) over 200 and 160 communication rounds, respectively. Adding a single client notably improves global model accuracy, bringing it closer to the benchmark.

and D_2 are 60.3% and 64.5%, respectively, with dark count rates of approximately 18 Hz and 28 Hz. The time window length is set to 1.8 ns. For Alice and Bob, we adjusted the attenuation values by attenuators between the users to make the total channel loss 6 dB, while for other client pairs, the total channel loss is set to 12 dB. The attenuation values are adjusted to ensure the channels are symmetric.

Our network design offers enhanced scalability and cost efficiency for QKD. In this setup, a Sagnac loop is employed to stabilize the phases among different users. The laser source and single-photon detectors are positioned at the party, Eve, outside the loop. Regardless of the number of clients, only one Eve is required for detection, thereby reducing the demand for measurement devices. Clients in this structure are only required to perform phase modulation on weak coherent states, eliminating the need for complex quantum state preparation and measurement. This design also allows for easy adjustment of the number of users. Adding or removing a user does not require any modifications to the detection terminal. For users already in the network, when they need to begin the key generation process, they only need to increase or decrease the fiber length to avoid collisions of pulses in both clockwise and counterclockwise directions.

The probability of choosing the X basis is 90% during implementation and the period length of random number is 10000. Error rates varied across different user pairs, prompting us to use a genetic algorithm to optimize the key rate for each pair under these differing error conditions. This optimization led to variations in pulse in-

tensity across pairs. To ensure an adequate supply of secret keys, we collected data continuously for 200 seconds, enabling quantum-secure collaborative learning for all participating clients in the following. For the 3-client scenario, the keys can train a model with 1434 parameters (floating-point numbers with 32-bit precision, 200 communication rounds), while for the 4-client scenario, the number of parameters is 1393. Key rates for different pairs of clients are presented in Table I. Details about simulation and post-processing can be seen in Methods.

Evaluation on QNN classifying quantum datasets.

Detecting and certifying quantum resources, such as entanglement and quantum magic (nonstabilizerness), is essential in practical quantum technologies [54–57]. In this context, we utilized the QuNetQFL in an IID setting, employing QNN with a hardware-efficient ansatz (HEA) [58] to classify both high and low multipartite entangled states, as well as non-stabilizer and stabilizer states from two distinct quantum datasets respectively. Comprehensive details of the datasets and simulations are provided in the Methods section. Utilizing experimentally generated secret keys for quantum-secure aggregation, we demonstrated secure collaborative learning capabilities across three and four-client scenarios. Figure 3 illustrates comparative performances in these scenarios using 16-bit quantization ($q = 16$), against an ideal benchmark where all client data is centrally processed. The results highlight a notable improvement in the global model’s test accuracy with the addition of a single client in both classification tasks, aligning it more closely with the benchmark’s performance. This finding

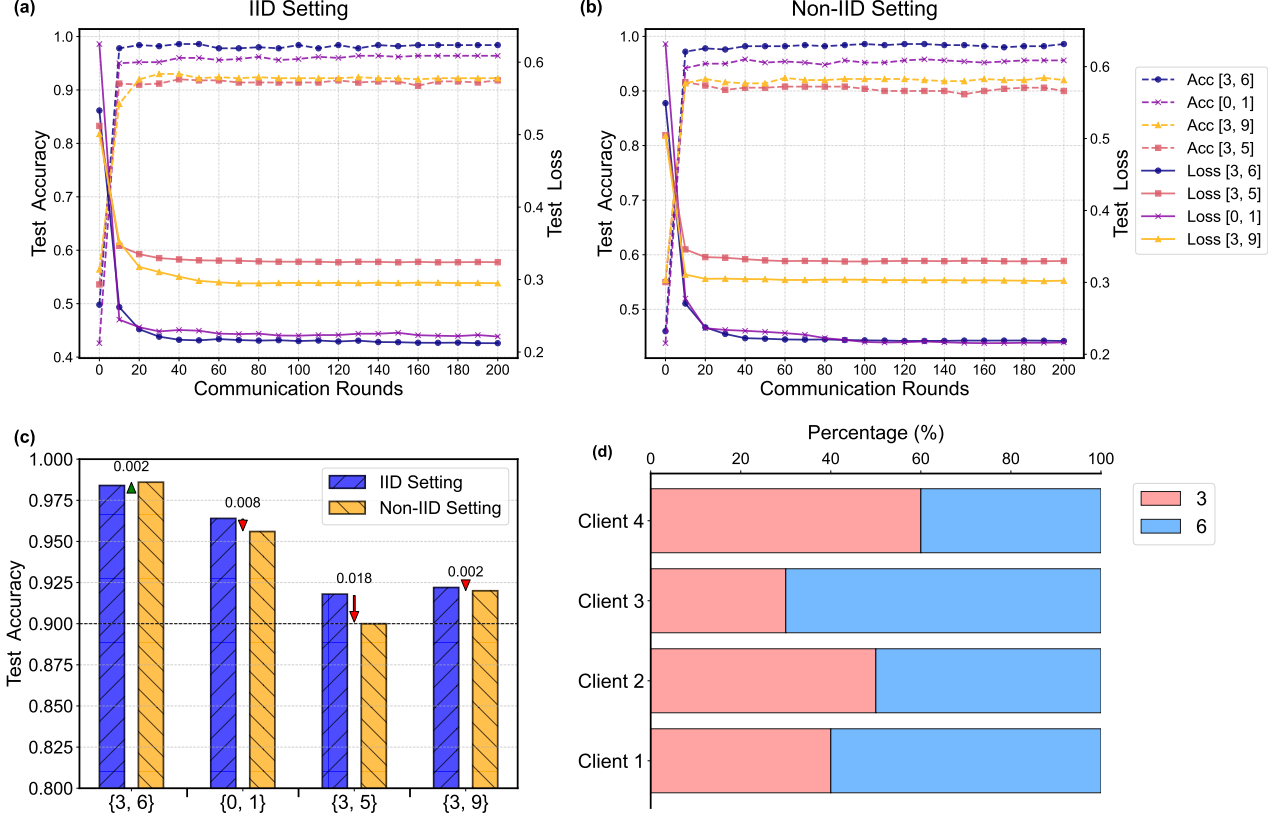


Fig 4. **Evaluation of QuNetQFL on the MNIST classification task using QNN.** (a) IID setting showing test accuracy and loss across 200 communication rounds for client combinations $\{3, 6\}$, $\{0, 1\}$, $\{3, 5\}$, and $\{3, 9\}$ with 16-bit quantization. (b) Non-IID setting with identical client configurations as (a) for comparative analysis. (c) Final test accuracy comparison between IID and non-IID settings, with annotated accuracy differences illustrating QuNetQFL’s robustness across data distributions. (d) Non-IID client data distribution proportions for classes $\{3, 6\}$ (same for other cases), highlighting dataset heterogeneity.

underscores the framework’s scalability and its promise for advancing secure and effective collaborative learning among several quantum data centers [59] in quantum network environments. Note that all QNNs in this work were implemented through the PennyLane library [60].

Evaluation on QNN classifying MNIST. To demonstrate the robustness and adaptability of QuNetQFL in real-world, heterogeneous data environments, we evaluated its performance across both IID and non-IID settings for four clients using QNNs on the classical MNIST dataset. We created multiple two-class subsets from MNIST, specifically $\{3, 6\}$, $\{0, 1\}$, $\{3, 9\}$, and $\{3, 5\}$, where, for instance, $\{3, 9\}$ represents images of digits “3” and “9”. Each client was allocated 500 training samples from the MNIST training set, while the server test set comprised 500 samples from the MNIST test set. In the IID setting, each client’s data contained an equal number of samples from each category. In contrast, the non-IID setting introduced imbalanced distributions to better reflect real-world scenarios where data varies across devices. The data splits among the four clients for

two classes were configured as (200, 300), (300, 200), (167, 333), and (333, 167), as shown in Fig. 4 (d). To accommodate quantum resource constraints, we resized the original 28×28 images to 4×4 and encoded each into 4-qubit states via amplitude embedding. The classification task utilized a 4-qubit QNN with a three-layer HEA, as shown in Fig. 1 (d). Results in Fig. 4 show rapid convergence of the test loss within the first 40 communication rounds for both IID and non-IID settings, as depicted in Fig. 4 (a) and (b). A comparison of final test accuracies across both data distributions, as shown in Fig. 4 (c), reveals close performance levels with a close communication time (≈ 40 rounds), highlighting the strong adaptability of our QFL framework across varying data distribution conditions.

Evaluation of the large-scale implementation of QuNetQFL. The QuNetQFL framework is flexible, supporting both quantum and classical machine learning models. If quantum computational resources are unavailable on either the clients or server, classical models can be used, ensuring scalability while benefiting from

TABLE II. Cost of quantum secret keys and test accuracy for 200 clients under different quantization levels.

	Cost (MB)	Accuracy
32-bit quantization	10.593	0.9798
16-bit quantization	5.296	0.9738
8-bit quantization	2.648	0.9704
Benchmark	-	0.9860

quantum-secure communication at scale, particularly in quantum metropolitan area networks.

To evaluate the scalability of QuNetQFL, we implemented it using the classical LeNet5 model (61706 parameters) and the MNIST dataset in an IID setting. The training set was equally divided among 200 clients, each receiving 300 instances randomly. In each aggregation round, the server randomly selected 5% of the clients. The total number of rounds was set to 200, and clients performed local training with 5 local epochs, a batch size of 32, and the Adam optimizer at a learning rate of 0.01. Due to limitations in our ability to implement such scale quantum networks, we used pseudo-random numbers as masks instead of true quantum secret keys in this experiment to illustrate the impact of quantization on reducing quantum secret key costs in QuNetQFL.

Table II presents results for $q = 8, 16, 32$ -bit quantization and plaintext aggregation (benchmark), showing the quantum secret key cost (related to model update size) and corresponding test accuracy. The results show that 8-bit quantization reduces the quantum key cost by 4 \times , and 16-bit quantization achieves a 2 \times reduction compared to 32-bit quantization in each communication round. Despite 200 clients, convergence occurred within 20 to 40 rounds, with consistent performance across quantization levels and benchmarks, leading to significant communication savings, lower key costs, and reduced time in real-world collaborative learning. This evaluation demonstrates the role of quantization techniques employed in the QuNetQFL for balancing model performance and communication efficiency for scalable quantum-enhanced federated learning.

Discussion

In this work, we propose QuNetQFL, a quantum federated learning framework that leverages practical quantum networks to ensure information-theoretically secure communication among clients during model updates. QKD is employed to generate quantum secret keys, which serve as one-time pads to encrypt local model updates. To reduce costs, the framework integrates advancing quantization techniques. Additionally, QuNetQFL is versatile and can integrate other model compression techniques, such as low-rank tensor compression, weight pruning, and knowledge distillation, to further reduce

Algorithm 1 Protocol of QuNetQFL

Input: The untrained global model parameters with θ^0 , The data size distribution of clients $\{n_k\}_{k=1}^K$, the number of iterations T , quantization bit length q , the specific QKD protocols.

Output: Trained global model parameters θ^*

Initialization: Randomly generate a set of T subsets $\{\mathcal{S}^t\}_{t=1}^T$, where each \mathcal{S}^t contains an equal number of client indices.

for each round $t \in [T]$ **do**

1) Select the subset of clients' indexes \mathcal{S}^t .

2) For each client $i \in \mathcal{S}^t$:

a) Update the local model and compute the local update: $\Delta\theta_i^t \leftarrow \theta_i^t - \theta^{t-1}$.

b) Perform an **MDI QKD protocol** (see Box 1) with each other connected clients in the \mathcal{S}^t in the underlying quantum networks, and generate masking vector:

$$\mathbf{m}_i^t \leftarrow \sum_{j \in \mathcal{S}^t, j \neq i} (-1)^{i>j} \cdot \text{QK}_{i,j}^t.$$

c) Compute masked and quantized local update:

$$\Delta\tilde{\theta}_i^t \leftarrow [Q^q(p_i^t \cdot \Delta\theta_i^t) + \mathbf{m}_i^t] \bmod 2^q.$$

3) Aggregate updates: $\Delta\theta^t \leftarrow \left[\sum_{i \in \mathcal{S}^t} \Delta\tilde{\theta}_i^t \right] \bmod 2^q$.

4) Update global model: $\theta^t \leftarrow \theta^{t-1} + D^q(\Delta\theta^t)$.

end for

Output the trained global model parameters θ^T .

communication and quantum secret key costs.

We experimentally validated this approach using a five-party quantum network, achieving quantum secret key generation with key rates exceeding 30 kbps in both 3-client and 4-client scenarios, underscoring the feasibility of this method. Notably, twin-field QKD, based on the Saganc loop used in our experimental scheme, can reach distances of up to 200 km [61], suggesting the potential of our experimental scheme for large-scale QFL applications in metropolitan quantum networks. The framework takes advantage of advancing quantum network technologies, providing a platform for demonstrating the capabilities of quantum networks in large-scale distributed learning systems.

Leveraging the generated quantum secret keys, we evaluated QuNetQFL on federated learning tasks with QNNs on both real-world classical and quantum datasets, demonstrating its applicability in the noisy intermediate-scale quantum era. We also evaluated the framework's scalability using classical models in multi-client scenarios, considering the scarcity of quantum computing devices. These results validate QuNetQFL as an effective solution for secure and scalable quantum federated learning, current quantum hardware limitations.

While this work does not explicitly showcase quantum advantages in reducing computational or communication complexity, it provides a practical solution for quantum-

secure federated learning. Our approach specifically addresses the privacy of shared local model updates, complementing other federated learning methods based on blind quantum computing or quantum homomorphic encryption [28, 30]. Future work will focus on reducing communication complexity by integrating these advanced quantum algorithms, balancing efficiency with practical implementation.

Box 1 | MDI QKD Protocol subroutine

for Each client (i, j) pairs in $\mathcal{S}^t \times \mathcal{S}^t$ **do**
 1) Randomly choose basis (X or Y) and prepare corresponding weak coherent states $\otimes_{k=1}^n |e^{i\varphi_k} \sqrt{\mu}\rangle$, where μ is the pulse intensity.
 2) Send the states to an untrusted node, Eve, for measurement.
 3) Decide whether to flip the bit according to the measurement outcome.
 4) Estimate bit error rate by clients' announcements.
 5) Perform postprocessing steps (error correction and privacy amplification) to generate enough final secure keys.

end for

Note: Secret keys used in QuNetQFL can be generated during training or pre-generated to the overall process time. MDI QKD reduces the quantum resources required for client participation, and QuNetQFL is flexible to emerging QKD techniques.

Although QuNetQFL was primarily evaluated on variational quantum circuit models for the noisy intermediate-scale quantum era, it is also adaptable to large-scale quantum machine learning models [62], making it relevant for future fault-tolerant quantum computing. We anticipate that this work will inspire the development of more practical and scalable QFL schemes, further advancing quantum technologies in distributed learning systems.

Methods

Protocol of QuNetQFL. The detailed protocol for QuNetQFL is provided in Algorithm 1. Importantly, QuNetQFL is designed to be flexible, allowing clients to choose their local training algorithms based on resource constraints and computational requirements. Clients can employ either gradient-based methods or alternative non-gradient-based methods to update local models, particularly when obtaining the gradients of the QNN circuit is expensive.

Quantization technique. To efficiently utilize the secret keys generated in quantum networks and further re-

duce the communication overhead, we employ a quantization technique in QuNetQFL, originally developed for homomorphic encryption [49] and later adapted for secure aggregation [63]. This method quantizes a scalar $s \in \mathbb{R}$ within $[-\beta, \beta]$ into a q -bit sign integer in the range $[-(2^{q-1} - 1), 2^{q-1} - 1]$ using the q -bit Quantizer $Q^q(s)$:

$$Q^q(s) = \text{sgn}(s) \cdot \text{Round}(\text{abs}(s) \cdot (2^{q-1} - 1) / \beta), \quad (6)$$

where $\text{sgn}(\cdot)$ is the sign function, $\text{abs}(\cdot)$ denotes the absolute value, and $\text{Round}(\cdot)$ maps the input to the nearest integer. The corresponding de-quantized process for a quantized valued v is given by:

$$D^q(v) = \text{sgn}(v) \cdot (\text{abs}(v) \cdot \beta / (2^{q-1} - 1)). \quad (7)$$

Quantization is performed on the client side for local model updates, while de-quantization is executed on the cloud server for the aggregated global model. Model parameters are clipped to the range $[-\beta, \beta]$ to ensure quantization accuracy. Note that to handle signs during de-quantization, the server employs the following adjustment: If $v > 2^{q-1} - 1$, it is updated as $v - 2^q$, otherwise, v remains unchanged.

Protocol of quantum network. We employed a four-phase MDI QKD protocol [43] between each pair of participants to generate quantum secret keys. To illustrate this process, we use the example of Alice and Bob with an untrusted third party, Eve. All other user pairs in the network follow this same protocol to obtain their quantum secret keys.

(1) Alice and Bob choose the X basis with the probability p_x and the Y basis with the probability p_y ($p_y = 1 - p_x$). For the X basis, they prepare $|e^{ik_x\pi} \sqrt{\mu}\rangle$ where k_x is the logic bit value ($k_x \in \{0, 1\}$) and μ is the pulse intensity. For the Y basis, they prepare $|e^{i(k_y+1/2)\pi} \sqrt{\mu}\rangle$ where k_y is the logic bit value ($k_y \in \{0, 1\}$).

(2) Eve performs measurements on the pulses with a 50 : 50 BS and two single-photon detectors and records the detection results. One and only one detector clicks are defined as an effective event.

(3) The above steps are repeated many times to accumulate sufficient data. Eve announces all effective events and the corresponding detector that clicks. For each effective event announced by Eve, if D_2 clicks, Bob flips his corresponding logic bit. Alice and Charlie retain only the logical bits from effective measurements, discarding others. Then they disclose their basis choices for effective events through authenticated classical channels.

(4) Alice and Bob announce all their bit values in the Y basis to calculate the quantum bit error rate E_b^y in the Y basis to estimate the phase error rate under the X basis E_p , and the number of counts n_x and n_y can also be obtained under X and Y bases, respectively.

(5) Alice and Bob perform error correction on the remaining keys under the X basis and privacy amplification to obtain the final secret keys.

Simulation details of MDI QKD protocol. The final key rate of MDI QKD [43] can be given by

$$l = n_x [1 - H(\bar{E}_p)] - \lambda_{\text{EC}} - \log_2 \frac{2}{\epsilon_{\text{EC}}} - \log_2 \frac{1}{4\epsilon_{\text{PA}}^2}, \quad (8)$$

where n_x is the number of total counts in the X basis and \bar{E}_p is the upper bound of phase error rate under the X basis. $\lambda_{\text{EC}} = n_x f H(E_b^x)$ is the leaked information during error correction, where f is the error correction efficiency, E_b^x is the bit error rate under the X basis and $H(x) = -x \log_2 x - (1-x) \log_2 (1-x)$ denotes the binary Shannon entropy. ϵ_{EC} and ϵ_{PA} are the failure probabilities for the error correction and privacy amplification, respectively and we set $\epsilon_{\text{EC}} = \epsilon_{\text{PA}} = 10^{-10}$.

E_b^x can be obtained from experimental results and E_p is bounded by the following inequality

$$1 - 2\Delta \leq \sqrt{E_b^y E_p} + \sqrt{(1 - E_b^y)(1 - E_p)}, \quad (9)$$

where $\Delta = (1 - |\langle \Psi_Y | \Psi_X \rangle|^2) / 2Q$. $Q = n_{\text{tot}} / N$ is the total gain, where n_{tot} is the number of detection events and N is the number of pulses sent. $|\Psi_X\rangle$ ($|\Psi_Y\rangle$) is the basis-dependent state under the X (Y) basis. The fidelity can be expressed as

$$\begin{aligned} \langle \Psi_X | \Psi_Y \rangle &= \frac{1}{4} [(1 - \mathbf{i}) \langle \sqrt{\mu} | \mathbf{i} \sqrt{\mu} \rangle + (1 - \mathbf{i}) \\ &\quad \langle -\sqrt{\mu} | -\mathbf{i} \sqrt{\mu} \rangle + (1 + \mathbf{i}) \langle \sqrt{\mu} | -\mathbf{i} \sqrt{\mu} \rangle \\ &\quad + (1 + \mathbf{i}) \langle -\sqrt{\mu} | \mathbf{i} \sqrt{\mu} \rangle]. \end{aligned} \quad (10)$$

Considering the finite-key effect, Kato's inequality [64] is utilized. The upper bound of the expectation value m_y^* is given by $m_y + \Delta_{n_y}$, where $m_y = n_y E_b^y$ represents the number of errors in the Y basis and $\Delta_{n_y} = \sqrt{\frac{1}{2} n_y \ln \epsilon_F^{-1}}$ with the failure probability $\epsilon_F = 10^{-10}$. $E_b^{y*} = m_y^* / n_y$ can be calculated and E_p^* can be derived according to Eq. 9. Thus we can get the number of phase errors $m_p^* = n_x E_p^*$ and \bar{m}_p can subsequently be estimated by the inequality. Consequently, we can get the upper bound of phase error rate $\bar{E}_p = \bar{m}_p / n_x$.

Error correction and privacy amplification. To obtain the final keys from the raw keys, error correction is required to rectify bit errors, and privacy amplification is needed to eliminate the possibility of information leakage.

The raw keys of the participants are transformed into fully correlated bit strings by error correction, utilizing the Cascade key agreement mechanism [65]. Initially, the participants divide their keys into blocks with a variable length, determined by the estimated bit error rate. Based on the recommendation of [66] and our optimization, we designated the block length as $0.7/E_b^x$ with a growth factor of 2 and performed a total of 4 rounds.

In the first round, the participants calculate and compare the parity check values for each block. Subsequently, they use a dichotomy method to rectify blocks with errors. Following these procedures, each block will only contain an even number (including 0) of error bits.

In the following rounds, the participants first shuffle their keys with pre-shared random numbers, then proceed with block division and dichotomy error correction. After identifying and correcting new error bits, the participants backtrack their bit strings by applying the inverse sequence of random numbers and rectify blocks from previous rounds that corresponding to error bits. This is necessary because, after correcting an erroneous bit, the corresponding blocks from previous rounds will contain an odd number of errors, requiring additional error correction. Therefore, the additional error correction in the corresponding blocks is achievable. Through the above methods, we have achieved a stable error correction coefficient of $f < 1.2$ for our experimental data according to [66].

After error correction, the keys of the participants become identical. However, the risk of information leakage remains. A privacy amplification process is required to compress the information and ensure confidentiality.

Our privacy amplification algorithm is based on the fast Fourier transform (FFT) and inverse fast Fourier transform (IFFT) [67]. The final key length r is determined through finite key analysis and the length of raw keys n . We use a random binary $(n-1)$ -bit string $[v_0, v_1, \dots, v_{n-2}]$ to construct a $r \times (n-r)$ Toeplitz matrix $V_{r \times (n-r)}$ and combine an $r \times r$ identity matrix with it horizontally to obtain a modified matrix

$$S_{r \times n} = \begin{bmatrix} 1 & & v_{r-1} & v_r & \cdots & v_{n-2} \\ & 1 & v_{r-2} & v_{r-1} & & v_{n-3} \\ & & \ddots & \vdots & \ddots & \vdots \\ & & & 1 & v_1 & & v_{n-r} \\ & & & & 1 & v_0 & v_1 & \cdots & v_{n-r-1} \end{bmatrix}. \quad (11)$$

Afterwards, $X_n = [x_0, x_1, \dots, x_{n-1}]'$ is defined as the vector of the raw keys and $Y_r = [y_0, y_1, \dots, y_{r-1}]'$ is defined as the vector of the final keys. There is:

$$Y_r = S_{r \times n} \times X_n = X_r + Y_r', \quad (12)$$

where Y_r' can be obtain by $D_n \otimes X_n'$ [68]. Eq. 13 represents a circulant matrix D_n extended from the Toeplitz matrix $V_{r \times (n-r)}$. The vector $X_n' = [0, \dots, 0, x_r, \dots, x_{n-1}]$ is obtained by setting the first r values of the vector X_n to zero. The calculation procedure is presented in Eq. 14.

$$D_n = \begin{bmatrix} P_{(n-r) \times r} & P_{(n-r) \times (n-r)} \\ P_{r \times r} & V_{r \times (n-r)} \end{bmatrix}, \quad (13)$$

$$\begin{aligned}
& \left[P_{(n-r) \times (n-r)} \times X_{n-r} \right] \\
& \quad Y_r' \\
& = D_n \otimes X_n' \\
& = \text{IFFT}[\text{FFT}(D_n) \cdot \text{FFT}(X_n')].
\end{aligned} \tag{14}$$

The privacy amplification method described above is applied to the experimental data, integrating the final key vector Y_r , resulting in a processing rate exceeding 10 Mbps.

Two quantum datasets. We introduced the details of two quantum datasets used to evaluate the performance of QuNetQFL in entanglement classification and nonstabilizerness classification tasks. Entanglement is a fundamental resource for quantum information processing tasks, especially in quantum communication. A given n -qubit state $|\psi\rangle$ is a product state if and only if $|\psi\rangle = \otimes_{i=1}^n |\psi_i\rangle$, otherwise, it is entangled. For this task, we employed the NTangled dataset [69] which quantifies multipartite entanglement using Concentratable Entanglement (CE), defined as $C(|\psi\rangle) = 1 - \frac{1}{2^n} \sum_{\alpha \in P} \text{Tr}[\rho_\alpha^2]$. Here, P is the power set of the set $\{1, 2, \dots, n\}$, and the ρ_α is the reduced density operator with respect to the index α . States with higher $C(|\psi\rangle)$ exhibit greater entanglement. Following the methods in Ref. [69], we generated a balanced 3-qubit dataset consisting of low (CE = 0.05) and high (CE = 0.35) entangled states using a six-layer HEA. In an IID setting, each client accessed 160 states for training, while the server processed 200 test states with equal proportions from the two classes in both 3-client and 4-client scenarios.

Quantum magic, or nonstabilizerness [70–72], is crucial for achieving quantum computational advantage be-

yond classical simulation [73]. Stabilizer states, generated by Clifford operations, are classically simulable, whereas non-stabilizer states possess quantum magic. For this task, we employed a popular magic measure, *stabilizer Rényi entropy* [74], to quantify nonstabilizerness. A balanced 3-qubit dataset was generated, comprising non-stabilizer states with *stabilizer Rényi entropy* greater than 1.5 (sampled Haar-randomly) and stabilizer states selected from the total of 1080 three-qubit stabilizer states. Each client accessed 120 training states, and the server processed 120 test states, with equal class proportions in both 3-client and 4-client scenarios.

For both classification tasks, we used QNNs with the HEA, as shown in Fig. 1 (c). To enhance the capacity of the learning model, we input the states parallelly twice and adopted a 6-qubit HEA with 4 layers. The label predictions were obtained by measuring the last qubit of the circuit on the Z basis. These two tasks were performed with 16-bit quantization ($q = 16$) over 200 and 160 communication rounds, respectively. Each client conducted local training with a batch size of 32, an initial learning rate of 0.01, and the Adam optimizer, employing mean squared error as the loss function, with one local epoch per round.

Acknowledgements

We gratefully acknowledge the supports from the National Natural Science Foundation of China (No. 12274223), the Fundamental Research Funds for the Central Universities and the Research Funds of Renmin University of China (No. 24XNKJ14), and the Program for Innovative Talents and Entrepreneurs in Jiangsu (No. JSSCRC2021484). We gratefully acknowledge the icons made by Iconjam, Pop Vectors, Fantasyou, kerismaker, Paul J. and juicy_fish from www.flaticon.com, which are used in Fig. 1.

-
- [1] Y. LeCun, Y. Bengio, and G. Hinton, Deep learning, *Nature* **521**, 436 (2015).
 - [2] L.-P. Cen, J. Ji, J.-W. Lin, S.-T. Ju, H.-J. Lin, T.-P. Li, Y. Wang, J.-F. Yang, Y.-F. Liu, S. Tan, *et al.*, Automatic detection of 39 fundus diseases and conditions in retinal photographs using deep neural networks, *Nat. Commun.* **12**, 4828 (2021).
 - [3] B. R. Kiran, I. Sobh, V. Talpaert, P. Mannion, A. A. Al Sallab, S. Yogamani, and P. Pérez, Deep reinforcement learning for autonomous driving: A survey, *IEEE Trans. Intell. Transp. Syst.* **23**, 4909 (2021).
 - [4] J. Jumper, R. Evans, A. Pritzel, T. Green, M. Figurnov, O. Ronneberger, K. Tunyasuvunakool, R. Bates, A. Židek, A. Potapenko, *et al.*, Highly accurate protein structure prediction with alphafold, *Nature* **596**, 583 (2021).
 - [5] A. Davies, P. Veličković, L. Buesing, S. Blackwell, D. Zheng, N. Tomašev, R. Tanburn, P. Battaglia, C. Blundell, A. Juhász, *et al.*, Advancing mathematics by guiding human intuition with ai, *Nature* **600**, 70 (2021).
 - [6] T. B. Brown, B. Mann, N. Ryder, M. Subbiah, J. Kaplan, P. Dhariwal, A. Neelakantan, P. Shyam, G. Sastry, A. Askell, S. Agarwal, A. Herbert-Voss, G. Krueger, T. Henighan, R. Child, A. Ramesh, D. M. Ziegler, J. Wu, C. Winter, C. Hesse, M. Chen, E. Sigler, M. Litwin, S. Gray, B. Chess, J. Clark, C. Berner, S. McCandlish, A. Radford, I. Sutskever, and D. Amodei, Language models are few-shot learners, in *Proceedings of the 34th International Conference on Neural Information Processing Systems*, NIPS '20 (Curran Associates Inc., Red Hook, NY, USA, 2020).
 - [7] S. Milano, J. A. McGrane, and S. Leonelli, Large language models challenge the future of higher education, *Nat. Mach. Intell.* **5**, 333 (2023).
 - [8] J. Kaplan, S. McCandlish, T. Henighan, T. B. Brown, B. Chess, R. Child, S. Gray, A. Radford, J. Wu, and D. Amodei, *Scaling laws for neural language models*

- (2020), [arXiv:2001.08361 \[cs.LG\]](#).
- [9] D. Grishin, K. Obbad, and G. M. Church, Data privacy in the age of personal genomics, *Nat. Biotechnol.* **37**, 1115 (2019).
- [10] W. N. Price and I. G. Cohen, Privacy in the age of medical big data, *Nat. Med.* **25**, 37 (2019).
- [11] B. McMahan, E. Moore, D. Ramage, S. Hampson, and B. A. y. Arcas, Communication-Efficient Learning of Deep Networks from Decentralized Data, in *Proceedings of the 20th International Conference on Artificial Intelligence and Statistics*, Proceedings of Machine Learning Research, Vol. 54, edited by A. Singh and J. Zhu (PMLR, 2017) pp. 1273–1282.
- [12] Q. Yang, Y. Liu, T. Chen, and Y. Tong, Federated machine learning: Concept and applications, *ACM Transactions on Intelligent Systems and Technology (TIST)* **10**, 1 (2019).
- [13] N. Rieke, J. Hancox, W. Li, F. Milletari, H. R. Roth, S. Albarqouni, S. Bakas, M. N. Galtier, B. A. Landman, K. Maier-Hein, *et al.*, The future of digital health with federated learning, *npj Digital Med.* **3**, 119 (2020).
- [14] Y. Zhao, J. Zhao, M. Yang, T. Wang, N. Wang, L. Lyu, D. Niyato, and K.-Y. Lam, Local differential privacy-based federated learning for internet of things, *IEEE Internet Things J.* **8**, 8836 (2020).
- [15] L. Yang, B. Tan, V. W. Zheng, K. Chen, and Q. Yang, Federated recommendation systems, *Federated Learning: Privacy and Incentive*, 225 (2020).
- [16] J. Biamonte, P. Wittek, N. Pancotti, P. Rebentrost, N. Wiebe, and S. Lloyd, Quantum machine learning, *Nature* **549**, 195 (2017).
- [17] M. Cerezo, G. Verdon, H.-Y. Huang, L. Cincio, and P. J. Coles, Challenges and opportunities in quantum machine learning, *Nat. Comput. Sci.* **2**, 567 (2022).
- [18] M.-G. Zhou, Z.-P. Liu, H.-L. Yin, C.-L. Li, T.-K. Xu, and Z.-B. Chen, Quantum neural network for quantum neural computing, *Research* **6**, 0134 (2023).
- [19] C. Ren, H. Yu, R. Yan, M. Xu, Y. Shen, H. Zhu, D. Niyato, Z. Y. Dong, and L. C. Kwek, Towards quantum federated learning, [arXiv preprint arXiv:2306.09912](#) (2023).
- [20] S. Y.-C. Chen and S. Yoo, Federated quantum machine learning, *Entropy* **23**, 460 (2021).
- [21] A. S. Bhatia, S. Kais, and M. A. Alam, Federated quantum neural network: a new paradigm for collaborative quantum learning, *Quantum Sci. Technol.* **8**, 045032 (2023).
- [22] H. Zhao, Non-iid quantum federated learning with one-shot communication complexity, *Quantum Mach. Intell.* **5**, 3 (2023).
- [23] M. Cerezo, A. Arrasmith, R. Babbush, S. C. Benjamin, S. Endo, K. Fujii, J. R. McClean, K. Mitarai, X. Yuan, L. Cincio, *et al.*, Variational quantum algorithms, *Nat. Rev. Phys.* **3**, 625 (2021).
- [24] J. Preskill, Quantum computing in the nisq era and beyond, *Quantum* **2**, 79 (2018).
- [25] V. Mothukuri, R. M. Parizi, S. Pouriyeh, Y. Huang, A. Dehghantanha, and G. Srivastava, A survey on security and privacy of federated learning, *Future Gener. Comput. Syst.* **115**, 619 (2021).
- [26] Y. Zhang, C. Zhang, C. Zhang, L. Fan, B. Zeng, and Q. Yang, Federated learning with quantum secure aggregation, [arXiv preprint arXiv:2207.07444](#) (2022).
- [27] C. Li, N. Kumar, Z. Song, S. Chakrabarti, and M. Pistoia, Privacy-preserving quantum federated learning via gradient hiding, *Quantum Sci. Technol.* **9**, 035028 (2024).
- [28] W. Li and D.-L. Deng, Quantum delegated and federated learning via quantum homomorphic encryption (2024), [arXiv:2409.19359 \[quant-ph\]](#).
- [29] C. Li, B. Li, O. Amer, R. Shaydulin, S. Chakrabarti, G. Wang, H. Xu, H. Tang, I. Schoch, N. Kumar, *et al.*, Blind quantum machine learning with quantum bipartite correlator, *Phys. Rev. Lett.* **133**, 120602 (2024).
- [30] W. Li, S. Lu, and D.-L. Deng, Quantum federated learning through blind quantum computing, *Sci. China Phys., Mech. Astron.* **64**, 100312 (2021).
- [31] S. Wehner, D. Elkouss, and R. Hanson, Quantum internet: A vision for the road ahead, *Science* **362**, eaam9288 (2018).
- [32] H.-L. Yin, Y. Fu, C.-L. Li, C.-X. Weng, B.-H. Li, J. Gu, Y.-S. Lu, S. Huang, and Z.-B. Chen, Experimental quantum secure network with digital signatures and encryption, *Natl. Sci. Rev.* **10**, nwc228 (2023).
- [33] K. Azuma, S. E. Economou, D. Elkouss, P. Hilaire, L. Jiang, H.-K. Lo, and I. Tzitrin, Quantum repeaters: From quantum networks to the quantum internet, *Rev. Mod. Phys.* **95**, 045006 (2023).
- [34] S. Hermans, M. Pompili, H. Beukers, S. Baier, J. Borregaard, and R. Hanson, Qubit teleportation between non-neighbouring nodes in a quantum network, *Nature* **605**, 663 (2022).
- [35] X. Jing, C. Qian, C.-X. Weng, B.-H. Li, Z. Chen, C.-Q. Wang, J. Tang, X.-W. Gu, Y.-C. Kong, T.-S. Chen, *et al.*, Experimental quantum byzantine agreement on a three-user quantum network with integrated photonics, *Sci. Adv.* **10**, eadp2877 (2024).
- [36] P. Schiavsky, J. Kalb, E. Szatecsny, M.-C. Roehsner, T. Guggemos, A. Trenti, M. Bozzio, and P. Walther, Demonstration of quantum-digital payments, *Nat. Commun.* **14**, 3849 (2023).
- [37] S. Daiss, S. Langenfeld, S. Welte, E. Distant, P. Thomas, L. Hartung, O. Morin, and G. Rempe, A quantum-logic gate between distant quantum-network modules, *Science* **371**, 614 (2021).
- [38] X.-Y. Cao, B.-H. Li, Y. Wang, Y. Fu, H.-L. Yin, and Z.-B. Chen, Experimental quantum e-commerce, *Sci. Adv.* **10**, eadk3258 (2024).
- [39] H.-K. Lo, M. Curty, and B. Qi, Measurement-device-independent quantum key distribution, *Phys. Rev. Lett.* **108**, 130503 (2012).
- [40] M. Lucamarini, Z. L. Yuan, J. F. Dynes, and A. J. Shields, Overcoming the rate–distance limit of quantum key distribution without quantum repeaters, *Nature* **557**, 400 (2018).
- [41] Y.-M. Xie, Y.-S. Lu, C.-X. Weng, X.-Y. Cao, Z.-Y. Jia, Y. Bao, Y. Wang, Y. Fu, H.-L. Yin, and Z.-B. Chen, Breaking the rate-loss bound of quantum key distribution with asynchronous two-photon interference, *PRX Quantum* **3**, 020315 (2022).
- [42] S. Wang, Z.-Q. Yin, D.-Y. He, W. Chen, R.-Q. Wang, P. Ye, Y. Zhou, G.-J. Fan-Yuan, F.-X. Wang, W. Chen, *et al.*, Twin-field quantum key distribution over 830-km fibre, *Nat. Photonics* **16**, 154 (2022).
- [43] J. Gu, X.-Y. Cao, Y. Fu, Z.-W. He, Z.-J. Yin, H.-L.

- Yin, and Z.-B. Chen, Experimental measurement-device-independent type quantum key distribution with flawed and correlated sources, *Sci. Bull.* **67**, 2167 (2022).
- [44] L. Zhou, J. Lin, Y.-M. Xie, Y.-S. Lu, Y. Jing, H.-L. Yin, and Z. Yuan, Experimental quantum communication overcomes the rate-loss limit without global phase tracking, *Phys. Rev. Lett.* **130**, 250801 (2023).
- [45] Y. Liu, W.-J. Zhang, C. Jiang, J.-P. Chen, C. Zhang, W.-X. Pan, D. Ma, H. Dong, J.-M. Xiong, C.-J. Zhang, *et al.*, Experimental twin-field quantum key distribution over 1000 km fiber distance, *Phys. Rev. Lett.* **130**, 210801 (2023).
- [46] M. Chehimi, S. Y.-C. Chen, W. Saad, D. Towsley, and M. Debbah, Foundations of quantum federated learning over classical and quantum networks, *IEEE Network* (2023).
- [47] L. U. Khan, W. Saad, Z. Han, E. Hossain, and C. S. Hong, Federated learning for internet of things: Recent advances, taxonomy, and open challenges (2021), [arXiv:2009.13012 \[cs.NI\]](https://arxiv.org/abs/2009.13012).
- [48] Y. Aono, T. Hayashi, L. Wang, S. Moriai, *et al.*, Privacy-preserving deep learning via additively homomorphic encryption, *IEEE Trans. Inf. Forensics Secur.* **13**, 1333 (2017).
- [49] C. Zhang, S. Li, J. Xia, W. Wang, F. Yan, and Y. Liu, Batchcrypt: efficient homomorphic encryption for cross-silo federated learning, in *2020 USENIX annual technical conference (USENIX ATC 20)* (2020) pp. 493–506.
- [50] C. Chu, L. Jiang, and F. Chen, *Cryptoqfl: Quantum federated learning on encrypted data* (2023), [arXiv:2307.07012 \[quant-ph\]](https://arxiv.org/abs/2307.07012).
- [51] K. Bonawitz, V. Ivanov, B. Kreuter, A. Marcedone, H. B. McMahan, S. Patel, D. Ramage, A. Segal, and K. Seth, Practical secure aggregation for federated learning on user-held data (2016), [arXiv:1611.04482 \[cs.CR\]](https://arxiv.org/abs/1611.04482).
- [52] R. LaRose and B. Coyle, *c*, *Phys. Rev. A* **102**, 032420 (2020).
- [53] K. Bonawitz, V. Ivanov, B. Kreuter, A. Marcedone, H. B. McMahan, S. Patel, D. Ramage, A. Segal, and K. Seth, Practical secure aggregation for privacy-preserving machine learning, in *proceedings of the 2017 ACM SIGSAC Conference on Computer and Communications Security* (2017) pp. 1175–1191.
- [54] N. Friis, G. Vitagliano, M. Malik, and M. Huber, Entanglement certification from theory to experiment, *Nat. Rev. Phys.* **1**, 72–87 (2018).
- [55] J.-H. Cao, F. Chen, Q. Liu, T.-W. Mao, W.-X. Xu, L.-N. Wu, and L. You, Detection of entangled states supported by reinforcement learning, *Phys. Rev. Lett.* **131**, 073201 (2023).
- [56] C. Zhu, Z. Liu, C. Zhu, and X. Wang, Limitations of classically simulable measurements for quantum state discrimination, *Phys. Rev. Lett.* **133** (2024).
- [57] C. Zhu, C. Zhu, Z. Liu, and X. Wang, Entanglement cost of discriminating quantum states under locality constraints (2024), [arXiv:2402.18446 \[quant-ph\]](https://arxiv.org/abs/2402.18446).
- [58] A. Kandala, A. Mezzacapo, K. Temme, M. Takita, M. Brink, J. M. Chow, and J. M. Gambetta, Hardware-efficient variational quantum eigensolver for small molecules and quantum magnets, *Nature* **549**, 242 (2017).
- [59] J. Liu and L. Jiang, Quantum data center: Perspectives, *IEEE Network*, 1–1 (2024).
- [60] V. Bergholm, J. Izaac, M. Schuld, C. Gogolin, S. Ahmed, V. Ajith, M. S. Alam, G. Alonso-Linaje, B. Akash-Narayanan, A. Asadi, J. M. Arrazola, U. Azad, S. Banning, C. Blank, T. R. Bromley, B. A. Cordier, J. Ceroni, A. Delgado, O. D. Matteo, A. Dusko, T. Garg, D. Guala, A. Hayes, R. Hill, A. Ijaz, T. Isaacson, D. Ittah, S. Jahangiri, P. Jain, E. Jiang, A. Khandelwal, K. Kottmann, R. A. Lang, C. Lee, T. Loke, A. Lowe, K. McKiernan, J. J. Meyer, J. A. Montañez-Barrera, R. Moyard, Z. Niu, L. J. O’Riordan, S. Oud, A. Panigrahi, C.-Y. Park, D. Polatajko, N. Quesada, C. Roberts, N. Sá, I. Schoch, B. Shi, S. Shu, S. Sim, A. Singh, I. Strandberg, J. Soni, A. Száva, S. Thabet, R. A. Vargas-Hernández, T. Vincent, N. Vitucci, M. Weber, D. Wierichs, R. Wiersema, M. Willmann, V. Wong, S. Zhang, and N. Killoran, *Pennylane: Automatic differentiation of hybrid quantum-classical computations* (2022), [1811.04968 \[quant-ph\]](https://arxiv.org/abs/1811.04968).
- [61] R. Mandil, L. Qian, and H.-K. Lo, Long-fiber sagnac interferometers for twin field quantum key distribution networks, *arXiv preprint arXiv:2407.08009* (2024).
- [62] J. Liu, M. Liu, J.-P. Liu, Z. Ye, Y. Wang, Y. Alexeev, J. Eisert, and L. Jiang, Towards provably efficient quantum algorithms for large-scale machine-learning models, *Nat. Commun.* **15**, 434 (2024).
- [63] Y. Zheng, S. Lai, Y. Liu, X. Yuan, X. Yi, and C. Wang, Aggregation service for federated learning: An efficient, secure, and more resilient realization, *IEEE Transactions on Dependable and Secure Computing* **20**, 988 (2022).
- [64] G. Kato, Concentration inequality using unconfirmed knowledge, *arXiv preprint arXiv:2002.04357* (2020).
- [65] J. Martinez-Mateo, D. Elkouss, and V. Martin, Key reconciliation for high performance quantum key distribution, *Sci. Rep.* **3**, 1576 (2013).
- [66] C. Ye, S. Mathur, A. Reznik, Y. Shah, W. Trappe, and N. B. Mandayam, Information-theoretically secret key generation for fading wireless channels, *IEEE Trans. Inf. Forensics Secur.* **5**, 240 (2010).
- [67] B. Liu, B.-K. Zhao, W.-R. Yu, and C.-Q. Wu, Fit-pa: Fixed scale fft based privacy amplification algorithm for quantum key distribution, *JIT* **17**, 309 (2016).
- [68] Q. Li, B.-Z. Yan, H.-K. Mao, X.-F. Xue, Q. Han, and H. Guo, High-speed and adaptive fpga-based privacy amplification in quantum key distribution, *IEEE Access* **7**, 21482 (2019).
- [69] L. Schatzki, A. Arrasmith, P. J. Coles, and M. Cerezo, Entangled datasets for quantum machine learning (2021), [arXiv:2109.03400 \[quant-ph\]](https://arxiv.org/abs/2109.03400).
- [70] M. Howard and E. Campbell, Application of a Resource Theory for Magic States to Fault-Tolerant Quantum Computing, *Phys. Rev. Lett.* **118** (2017), 1609.07488.
- [71] X. Wang, M. M. Wilde, and Y. Su, Quantifying the magic of quantum channels, *New J. Phys.* **21**, 103002 (2019).
- [72] J. R. Seddon, B. Regula, H. Pashayan, Y. Ouyang, and E. T. Campbell, Quantifying Quantum Speedups: Improved Classical Simulation From Tighter Magic Monotones, *PRX Quantum* **2**, 010345 (2021).
- [73] D. Gottesman, *Stabilizer codes and quantum error correction* (California Institute of Technology, 1997).
- [74] L. Leone, S. F. Oliviero, and A. Hama, Stabilizer Rényi Entropy, *Phys. Rev. Lett.* **128** (2022).

Supplementary Information: Practical quantum federated learning and its experimental demonstration

CONTENTS

I. Convergence analysis	1
II. Quantum Neural Network Model	5
III. Evaluation on Quantum neural networks classifying MNIST	6
IV. Evaluation of the large-scale implementation of QuNetQFL	7
V. Detailed experimental data of quantum networks	8
References	9

I. CONVERGENCE ANALYSIS

In this section, we provide a theoretical convergence analysis for our quantum federated learning framework (QuNetQFL) under the use of a gradient-based optimization algorithm. The analysis begins with the introduction of four key assumptions and concludes with Theorem S1, which formalizes the convergence behavior of the framework.

Consider round t of our federated learning process, where the global model parameters are denoted by $\boldsymbol{\theta}^t \in \mathbb{R}^M$. At each round, K clients are selected to update the model locally. Each client receives the global model and performs τ iterations of local gradient descent, starting from $\boldsymbol{\theta}_k^{t,0} = \boldsymbol{\theta}^t$. The local update for k -th client is given by:

$$\boldsymbol{\theta}_k^{t,s+1} = \boldsymbol{\theta}_k^{t,s} - \eta g(\boldsymbol{\theta}_k^{t,s}; \xi_k^{t,s}), \quad s = 0, 1, \dots, \tau - 1, \quad (\text{S1})$$

where η is the learning rate and $\xi_k^{t,s}$ denotes the mini-batch of data sampled from the k -th client's local data at iteration s . After τ iterations, client k obtains the updated parameters $\boldsymbol{\theta}_k^{t,\tau}$. Next, the client computes the parameter difference $\Delta \boldsymbol{\theta}_k^t = \boldsymbol{\theta}_k^{t,\tau} - \boldsymbol{\theta}^t$, clips it to the range $[-\beta, \beta]$, and quantizes it into q bits. Next, the client then adds a privacy mask \mathbf{m}_k^t and sends the masked update $\Delta \tilde{\boldsymbol{\theta}}_k^t = [Q^q(p_k \Delta \boldsymbol{\theta}_k^t) + \mathbf{m}_k^t] \bmod 2^q$ to the server.

On the server side, the aggregated model update is computed as follows:

$$\begin{aligned} \boldsymbol{\theta}^{t+1} &= \boldsymbol{\theta}^t + D^q \left(\sum_{k=1}^K \Delta \tilde{\boldsymbol{\theta}}_k^t \right) \\ &= \boldsymbol{\theta}^t + D^q \left(\sum_{k=1}^K [Q^q(p_k \Delta \boldsymbol{\theta}_k^t) + \mathbf{m}_k^t] \bmod 2^q \right) \end{aligned} \quad (\text{S2})$$

where $p_k = \frac{n_k}{N}$, with n_k denoting the number of local data samples held by the k -th client, and N representing the total number of data samples across all participating clients. Here, $Q^q(\cdot)$ is the q -bit quantization function, and $D^q(\cdot)$ is the corresponding q -bit dequantization function. The masking terms \mathbf{m}_k^t does not affect the final aggregated result, since $[\sum_k \mathbf{m}_k^t] \bmod 2^q = 0$.

The objective is to solve the following optimization problem:

$$\min_{\boldsymbol{\theta} \in \mathbb{R}^M} f(\boldsymbol{\theta}) = \sum_{k=1}^K p_k f_k(\boldsymbol{\theta}), \quad (\text{S3})$$

where $f_k(\boldsymbol{\theta}) = \mathbb{E}_{\xi \sim \mathcal{D}_k} [f_k(\boldsymbol{\theta}; \xi)]$ is the loss function of the k -th client, and \mathcal{D}_k represents the local data distribution for client k .

Next, we outline the assumptions typically used in the convergence analysis of federated learning [1–4].

Assumption I.1 *The loss function f_k is μ -strongly convex and satisfies the Polyak-Lojasiewicz (PL) inequality [5]:*

$$2\mu(f_k(\boldsymbol{\theta}) - f^*) \leq \|\nabla f_k(\boldsymbol{\theta})\|_2^2,$$

for any $\boldsymbol{\theta}$, where f^* denotes the global optimum.

Assumption I.2 *The loss function f_k is L -smooth with a Lipschitz constant $L > 0$. That is, for any $\boldsymbol{\theta}_1, \boldsymbol{\theta}_2$, the following inequality holds:*

$$f_k(\boldsymbol{\theta}_2) \leq f_k(\boldsymbol{\theta}_1) + \nabla f_k(\boldsymbol{\theta}_1)^T (\boldsymbol{\theta}_2 - \boldsymbol{\theta}_1) + \frac{L}{2} \|\boldsymbol{\theta}_2 - \boldsymbol{\theta}_1\|^2.$$

Assumption I.3 *The stochastic gradient $g(\boldsymbol{\theta}_k^{t,s}) = \nabla f(\boldsymbol{\theta}_k^{t,s})$ is unbiased and bounded. Specifically,*

$$\mathbb{E}_{\xi \sim \mathcal{D}_k} [g(\boldsymbol{\theta}_k^{t,s})] = \nabla f_k(\boldsymbol{\theta}_k^{t,s}), \quad \text{and} \quad \text{Var}(\nabla f(\boldsymbol{\theta}_k^{t,s})) \leq \sigma^2,$$

where the mini-batch gradient $g(\boldsymbol{\theta}_k^{t,s})$ is defined as $g(\boldsymbol{\theta}_k^{t,s}) = \frac{1}{b} \sum_{j=1}^b \nabla f(\boldsymbol{\theta}_k^{t,s}; \xi_k^{t,s,j})$ and b is the mini-batch size. Based on these assumptions, the expected squared norm of the mini-batch gradient is bounded as follows:

$$\mathbb{E}[\|g(\boldsymbol{\theta}_k^{t,s})\|^2] \leq \|\nabla f_k(\boldsymbol{\theta}_k^{t,s})\|^2 + \frac{\sigma^2}{b}.$$

Assumption I.4 *For a parameter $\Delta\boldsymbol{\theta}_m$ in $\Delta\boldsymbol{\theta}_k^t$, the quantized result $Q(\Delta\boldsymbol{\theta}_m)$ satisfies: $Q(\Delta\boldsymbol{\theta}_m) = \Delta\boldsymbol{\theta}_m + \omega$, where ω is a random variable distributed as $\omega \sim U(-\delta_q, \delta_q)$ with $\delta_q = \frac{\beta}{2^{q-1}-1}$, and $U(\cdot)$ denotes the uniform random distribution. Thus, for the entire parameter $\Delta\boldsymbol{\theta}_k^t$, the quantized result is $Q(\Delta\boldsymbol{\theta}_k^t) = \Delta\boldsymbol{\theta}_k^t + \Omega$, where Ω is an M -dimensional vector, with each component independently distributed as $U(-\delta_q, \delta_q)$.*

Theorem S1 *Under the assumptions above, if the server and clients update the global model $\boldsymbol{\theta}^t \in \mathbb{R}^M$ following the described protocol, and the learning rate η satisfies $\eta \leq \frac{1}{L}$, the expected convergence of the global loss function after T rounds of training is bounded by:*

$$\mathbb{E}[f(\boldsymbol{\theta}^T)] - f^* \leq (1 - \eta\mu)^{T\tau} (\mathbb{E}[f(\boldsymbol{\theta}^0)] - f^*) + [1 - (1 - \eta\mu)^{T\tau}] [E_g + \frac{E_q}{1 - (1 - \eta\mu)^\tau}] \quad (\text{S4})$$

where $E_g = \frac{\kappa\eta\sigma^2}{2b}$ with $\kappa = L/\mu$ being the condition number, and $E_q = \frac{LMK^2\delta_q^2}{6}$.

Proof

The global model aggregated by the sever at the $(t + 1)$ -th round is given as:

$$\begin{aligned}
\boldsymbol{\theta}^{t+1} &= \boldsymbol{\theta}^t + D^q \left(\sum_{k=1}^K [Q^q(p_k \Delta \boldsymbol{\theta}_k^t) + \mathbf{m}_k^t] \bmod 2^q \right) \\
&= \boldsymbol{\theta}^t + \sum_{k=1}^K (p_k \Delta \boldsymbol{\theta}_k^t + \Omega) \\
&= \sum_{k=1}^K p_k \boldsymbol{\theta}_k^{t,\tau} + K \cdot \Omega
\end{aligned} \tag{S5}$$

where the sum of the masking item equals zero, and the second equation comes from the Assumption I.4.

Define $\bar{\boldsymbol{\theta}}^{t+1} = \sum_{k=1}^K p_k \boldsymbol{\theta}_k^{t,\tau}$, we have

$$\mathbb{E}[\boldsymbol{\theta}^{t+1}] = \sum_{k=1}^K p_k \boldsymbol{\theta}_k^{t,\tau} = \bar{\boldsymbol{\theta}}^{t+1} \tag{S6}$$

Using Assumption I.2 and set $\boldsymbol{\theta}_2 = \boldsymbol{\theta}^{t+1}$ and $\boldsymbol{\theta}_1 = \bar{\boldsymbol{\theta}}^{t+1}$, we have

$$f(\boldsymbol{\theta}^{t+1}) \leq f(\bar{\boldsymbol{\theta}}^{t+1}) + \nabla f(\bar{\boldsymbol{\theta}}^{t+1})^\top (K \cdot \Omega) + \frac{L}{2} \|K \cdot \Omega\|^2 \tag{S7}$$

Since $\mathbb{E}[\boldsymbol{\theta}^{t+1}] = \bar{\boldsymbol{\theta}}^{t+1}$, and $K \cdot \Omega$ is independent of $\nabla F(\bar{\boldsymbol{\theta}}^{t+1})$, taking the expectation gives:

$$\begin{aligned}
\mathbb{E}[f(\boldsymbol{\theta}^{t+1})] &\leq \mathbb{E}[f(\bar{\boldsymbol{\theta}}^{t+1})] + \frac{L}{2} \mathbb{E}[\|K \cdot \Omega\|^2] \\
&= \mathbb{E}[f(\bar{\boldsymbol{\theta}}^{t+1})] + \frac{L}{2} \frac{MK^2 \delta_q^2}{3}
\end{aligned} \tag{S8}$$

As the loss function f is convex, we have

$$f(\bar{\boldsymbol{\theta}}^{t+1}) = f\left(\sum_{k=1}^K p_k \boldsymbol{\theta}_k^{t,\tau}\right) \leq \sum_{k=1}^K p_k f_k(\boldsymbol{\theta}_k^{t,\tau}) \tag{S9}$$

and then

$$\mathbb{E}[f(\bar{\boldsymbol{\theta}}^{t+1})] \leq \sum_{k=1}^K p_k \mathbb{E}[f_k(\boldsymbol{\theta}_k^{t,\tau})] \tag{S10}$$

Locally, the client updates the parameters with stochastic gradient descent. Specifically, $\boldsymbol{\theta}_k^{t,s+1} = \boldsymbol{\theta}_k^{t,s} - \eta g(\boldsymbol{\theta}_k^{t,s}; \xi_k^{t,s})$. Using Assumption I.2, for client k

$$\begin{aligned}
f_k(\boldsymbol{\theta}_k^{t,s+1}) - f_k(\boldsymbol{\theta}_k^{t,s}) &\leq \nabla f_k(\boldsymbol{\theta}_k^{t,s})^\top (\boldsymbol{\theta}_k^{t,s+1} - \boldsymbol{\theta}_k^{t,s}) + \frac{L}{2} \|\boldsymbol{\theta}_k^{t,s+1} - \boldsymbol{\theta}_k^{t,s}\|^2 \\
&\leq -\eta \nabla f_k(\boldsymbol{\theta}_k^{t,s})^\top g(\boldsymbol{\theta}_k^{t,s}; \xi_k^{t,s}) + \frac{L}{2} \|\eta g(\boldsymbol{\theta}_k^{t,s}; \xi_k^{t,s})\|^2 \\
&= -\eta \nabla f_k(\boldsymbol{\theta}_k^{t,s})^\top g(\boldsymbol{\theta}_k^{t,s}; \xi_k^{t,s}) + \frac{L\eta^2}{2} \|g(\boldsymbol{\theta}_k^{t,s}; \xi_k^{t,s})\|^2
\end{aligned} \tag{S11}$$

After taking expectations on both sides and using Assumption I.3, what we have is the following:

$$\mathbb{E}[f_k(\boldsymbol{\theta}_k^{t,s+1}) - f_k(\boldsymbol{\theta}_k^{t,s})] \leq -\eta \|\nabla f_k(\boldsymbol{\theta}_k^{t,s})\|^2 + \frac{L\eta^2}{2} \|\nabla f_k(\boldsymbol{\theta}_k^{t,s})\|^2 + \frac{L\eta^2\sigma^2}{2b} \quad (\text{S12})$$

After simplification, we obtain:

$$\mathbb{E}[f_k(\boldsymbol{\theta}_k^{t,s+1}) - f_k(\boldsymbol{\theta}_k^{t,s})] = (\eta - \frac{L\eta^2}{2})(-\|\nabla f_k(\boldsymbol{\theta}_k^{t,s})\|^2) + \frac{L\eta^2\sigma^2}{2b} \quad (\text{S13})$$

If we choose $\eta \leq \frac{1}{L}$, then

$$\mathbb{E}[f_k(\boldsymbol{\theta}_k^{t,s+1})] - \mathbb{E}[f_k(\boldsymbol{\theta}_k^{t,s})] \leq \frac{\eta}{2}(-\|\nabla f_k(\boldsymbol{\theta}_k^{t,s})\|^2) + \frac{L\eta^2\sigma^2}{2b} \quad (\text{S14})$$

According to I.1, we have:

$$\|\nabla f_k(\boldsymbol{\theta}_k^{t,s})\|^2 \geq 2\mu(f_k(\boldsymbol{\theta}_k^{t,s}) - f^*) \quad (\text{S15})$$

As a result,

$$\mathbb{E}[f_k(\boldsymbol{\theta}_k^{t,s+1})] - \mathbb{E}[f_k(\boldsymbol{\theta}_k^{t,s})] \leq -\eta\mu(\mathbb{E}[f_k(\boldsymbol{\theta}_k^{t,s})] - f^*) + \frac{L\eta^2\sigma^2}{2b} \quad (\text{S16})$$

By transforming the formula and iterating it for τ steps, while using $\boldsymbol{\theta}_k^{t,0} = \boldsymbol{\theta}^t$, we obtain:

$$\mathbb{E}[f_k(\boldsymbol{\theta}_k^{t,\tau})] - f^* - \frac{L\eta\sigma^2}{2\mu b} \leq (1 - \eta\mu)^\tau (\mathbb{E}[f_k(\boldsymbol{\theta}^t)] - f^* - \frac{L\eta\sigma^2}{2\mu b}) \quad (\text{S17})$$

Sum up all clients, we have

$$\sum_{k=1}^K p_k \mathbb{E}[f_k(\boldsymbol{\theta}_k^{t,\tau})] - f^* - \frac{L\eta\sigma^2}{2\mu b} \leq (1 - \eta\mu)^\tau (\mathbb{E}[f(\boldsymbol{\theta}^t)] - f^* - \frac{L\eta\sigma^2}{2\mu b}) \quad (\text{S18})$$

Combine Eq. (S8), Eq. (S10) and Eq. (S18), it is obvious that

$$\begin{aligned} \mathbb{E}[f(\boldsymbol{\theta}^{t+1})] &\leq \sum_{k=1}^K p_k \mathbb{E}[f_k(\boldsymbol{\theta}_k^{t,\tau})] + \frac{LMK^2\delta_q^2}{6} \\ &= (1 - \eta\mu)^\tau (\mathbb{E}[f(\boldsymbol{\theta}^t)] - f^* - \frac{L\eta\sigma^2}{2\mu b}) + f^* + \frac{L\eta\sigma^2}{2\mu b} + \frac{LMK^2\delta_q^2}{6} \end{aligned} \quad (\text{S19})$$

We denote the error item caused by batch gradient descent as $E_g = \frac{\kappa\eta\sigma^2}{2b}$ with $\kappa = L/\mu$ being the condition number, and $\frac{LMK^2\delta_q^2}{6}$ as the error E_q caused by quantization. Therefore, we have the following relationship:

$$\mathbb{E}[f(\boldsymbol{\theta}^{t+1})] - f^* - \left[E_g + \frac{E_q}{1 - (1 - \eta\mu)^\tau} \right] \leq (1 - \eta\mu)^\tau \left(\mathbb{E}[f(\boldsymbol{\theta}^t)] - f^* - \left[E_g + \frac{E_q}{1 - (1 - \eta\mu)^\tau} \right] \right) \quad (\text{S20})$$

After performing T rounds of training globally, the following equation can be obtained:

$$\mathbb{E}[f(\boldsymbol{\theta}^T)] - f^* - \left[E_g + \frac{E_q}{1 - (1 - \eta\mu)^\tau} \right] \leq (1 - \eta\mu)^{T\tau} \left(\mathbb{E}[f(\boldsymbol{\theta}^0)] - f^* - \left[E_g + \frac{E_q}{1 - (1 - \eta\mu)^\tau} \right] \right) \quad (\text{S21})$$

Then we arrive at the conclusion that

$$\mathbb{E}[f(\boldsymbol{\theta}^T)] - f^* \leq (1 - \eta\mu)^{T\tau} (\mathbb{E}[f(\boldsymbol{\theta}^0)] - f^*) + [1 - (1 - \eta\mu)^{T\tau}] \left[E_g + \frac{E_q}{1 - (1 - \eta\mu)^\tau} \right] \quad (\text{S22})$$

■

Asymptotic Convergence Analysis: In summary, the model converges to the optimal solution f^* over time, with the first term in the equation representing the exponential decay of the initial error. However, due to stochastic noise and quantization errors, the second term introduces a constant error floor. As a result, the error is upper-bounded by $E_g + \frac{E_q}{1 - (1 - \eta\mu)^\tau}$ as $T \rightarrow \infty$. Specifically, by adopting strategies to reduce the condition number κ and selecting an appropriate quantization precision relative to the model size, this asymptotic upper bound can be made small enough. Moreover, this asymptotic convergence analysis indicates restricting the number of selected clients in each round can accelerate the convergence of training in our QFL framework. This analysis not only provides a theoretical convergence guarantee but also offers practical guidance for training in the QuNetQFL framework, further highlighting its practical advantages.

II. QUANTUM NEURAL NETWORK MODEL

In this section, we briefly introduce the Quantum Neural Network (QNN) model [6], which uses a series of parameterized quantum gates to simulate classical neural network learning. Given a training dataset $\{\mathbf{x}_i, y_i\}_{i=1}^N$, classical input data $\mathbf{x}_i \in \mathbb{R}^d$ is encoded into an n -qubit quantum state $\rho(\mathbf{x}_i) = U_{\text{emb}}(\mathbf{x}_i) |0\rangle^{\otimes n} \langle 0|^{\otimes n} U_{\text{emb}}^\dagger(\mathbf{x}_i)$ in a QNN, where $U_{\text{emb}}(\mathbf{x}_i)$ is a unitary embedding operator. The common encoding strategies include amplitude encoding, and angle encoding [7, 8]. The quantum state is processed by a series of parameterized quantum gates $U(\boldsymbol{\theta})$, with $\boldsymbol{\theta}$ as the trainable parameters.

The output is measured using an observable operator O , and the model's prediction $E(\boldsymbol{\theta})$ is the expectation value of the observable:

$$E(\boldsymbol{\theta}) = \text{Tr} \left[U(\boldsymbol{\theta}) U_{\text{emb}}(\mathbf{x}_i) |0\rangle^{\otimes n} \langle 0|^{\otimes n} U_{\text{emb}}^\dagger(\mathbf{x}_i) U^\dagger(\boldsymbol{\theta}) O \right] \quad (\text{S23})$$

QNNs are trained by minimizing a loss function $f(\boldsymbol{\theta})$, which quantifies the difference between the predicted outputs $E(\boldsymbol{\theta})$ and actual labels y . The loss function is optimized using gradient-based techniques, with gradients evaluated via the parameter shift rule [9].

III. EVALUATION ON QUANTUM NEURAL NETWORKS CLASSIFYING MNIST

In this section, we outline the specific parameter settings of numerical experiments for classifying MNIST via QNNs in Table I.

TABLE I. Parameter settings for classifying MNIST via QNN

Parameter	Non-IID (IID)
Num of qubits	4
Circuit layer	3
Training set (per client)	500
Test set (Server)	500
Optimizer	Adam
Learning rate	0.01
Batch size	50
Local epoch	1
Loss function	MSE

IV. EVALUATION OF THE LARGE-SCALE IMPLEMENTATION OF QUNETQFL

In this section, we present Fig S1, which illustrates the test accuracy and loss over 200 communication rounds for 200 clients, evaluated at different quantization levels. Despite the involvement of up to 200 clients in the collaborative learning process on the MNIST dataset, we observe a rapid convergence within approximately 20 to 40 rounds, with consistent performance across various quantization levels and the benchmark. This demonstrates the efficiency and scalability of QuNetQFL in real-world datasets, achieving rapid convergence and consistent performance even in large-scale, distributed quantum-enhanced learning environments.

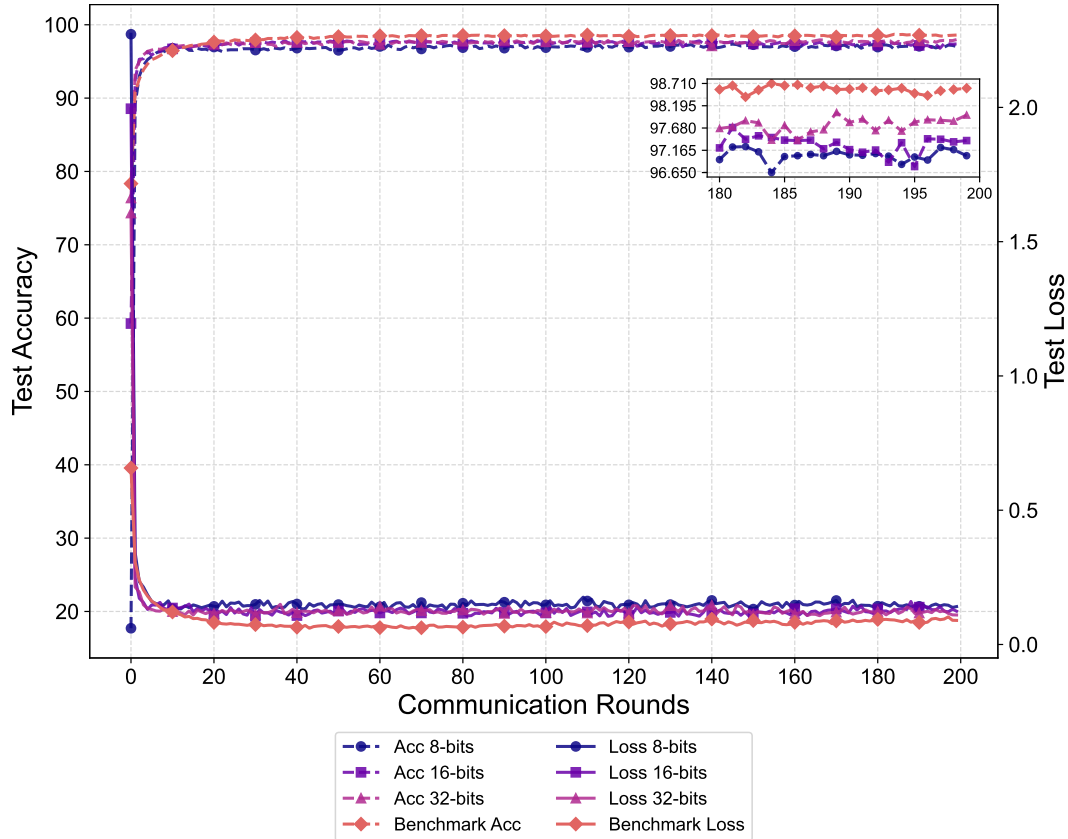


Fig S1. Test accuracy and loss across 200 communication rounds for 200 clients, evaluated at different quantization levels.

V. DETAILED EXPERIMENTAL DATA OF QUANTUM NETWORKS

In this section, we present the calibrated efficiencies of the devices in Eve’s site in Table II. The insertion losses of four users (Alice, Bob, Charlie, and David) are 3.62 dB, 3.08 dB, 3.16 dB and 3.01 dB, respectively. Table III records the corresponding data used for key rate calculation.

TABLE II. **The efficiencies of devices.**

Optical element	Efficiency
Cir 2→3	89.3%
BS-1	84.7%
BS-2	85.5%
PC ₁	92.7%
PC ₂	90.1%

TABLE III. **Summary of experimental data.** The total number of detector clicks, n_{tot} , includes the clicks under the X basis (n_x), the Y basis (n_y), and the detection events corresponding to phase differences that are odd multiples of $\pi/2$. m_x (m_y) represents the number of detection errors under the X (Y) basis. E_b^x and E_b^y represent the bit error rate under the X basis and under the Y basis, respectively. λ_{EC} is the leaked information during error correction. A, B, C, and D represent Alice, Bob, Charlie, and David, respectively.

	Client pair	Intensity	n_{tot}	n_x	m_x	n_y	m_y	E_b^x	E_b^y	λ_{EC}
3-client	AB	0.017	208796444	169216602	1434989	2171543	10748	0.85%	0.49%	14220217
	AC	0.0085	52455918	42542127	446184	575833	7221	1.05%	1.25%	4219418
	AD	0.0089	54706564	44275485	437014	517003	3405	0.99%	0.66%	4221496
4-client	AB	0.017	209641454	169711875	1301843	2095785	8263	0.77%	0.39%	13122399
	AC	0.0083	51270791	41489668	463434	472642	6228	1.11%	1.32%	4378680
	AD	0.0087	53621226	43467119	439500	536452	4636	1.01%	0.86%	4234674
	BC	0.0087	53175349	43089366	429297	561109	4106	1.00%	0.73%	4139771
	BD	0.0087	53520583	43268936	478145	456832	5182	1.10%	1.13%	4520879
	CD	0.0074	45406632	36791065	530094	442536	5523	1.44%	1.25%	4720904

-
- [1] S. Chen, L. Li, G. Wang, M. Pang, and C. Shen, Federated learning with heterogeneous quantization bit allocation and aggregation for internet of things, *IEEE Internet Things J.* , **1** (2023).
 - [2] M. M. Amiri, D. Gunduz, S. R. Kulkarni, and H. V. Poor, Federated learning with quantized global model updates (2020), [arXiv:2006.10672 \[cs.IT\]](https://arxiv.org/abs/2006.10672).
 - [3] P. Jiang and G. Agrawal, A linear speedup analysis of distributed deep learning with sparse and quantized communication, in *Advances in Neural Information Processing Systems*, Vol. 31, edited by S. Bengio, H. Wallach, H. Larochelle, K. Grauman, N. Cesa-Bianchi, and R. Garnett (Curran Associates, Inc., 2018).
 - [4] S. Bubeck *et al.*, Convex optimization: Algorithms and complexity, *Foundations and Trends® in Machine Learning* **8**, 231 (2015).
 - [5] H. Karimi, J. Nutini, and M. Schmidt, Linear convergence of gradient and proximal-gradient methods under the polyak-Łojasiewicz condition, in *Machine Learning and Knowledge Discovery in Databases: European Conference, ECML PKDD 2016, Riva del Garda, Italy, September 19-23, 2016, Proceedings, Part I 16* (Springer, 2016) pp. 795–811.
 - [6] M. Cerezo, A. Arrasmith, R. Babbush, S. C. Benjamin, S. Endo, K. Fujii, J. R. McClean, K. Mitarai, X. Yuan, L. Cincio, *et al.*, Variational quantum algorithms, *Nat. Rev. Phys.* **3**, 625 (2021).
 - [7] M. Schuld, R. Sweke, and J. J. Meyer, Effect of data encoding on the expressive power of variational quantum-machine-learning models, *Phys. Rev. A* **103**, 032430 (2021).
 - [8] R. LaRose and B. Coyle, Robust data encodings for quantum classifiers, *Phys. Rev. A* **102**, 032420 (2020).
 - [9] K. Mitarai, M. Negoro, M. Kitagawa, and K. Fujii, Quantum circuit learning, *Phys. Rev. A* **98**, 032309 (2018).